Cellular and Molecular Bioengineering (2023) 16:459–474
https://doi.org/10.1007/s12195-023-00784-w

BMES BIOMEDICAL ENGINEERING SOCIETY

ORIGINAL ARTICLE

Nuclear Entry of DNA and Transgene Expression in Dividing and Non-dividing Cells

Justin Sylvers[1] · **Yifei Wang**[1] · **Fan Yuan**[1]

Received: 2 February 2023 / Accepted: 3 September 2023 / Published online: 17 September 2023

Abstract

Introduction Plasmid DNA (pDNA) must be delivered into the nucleus for transgene expression in mammalian cells. The entry may happen passively during the nuclear envelope breakdown and reformation in dividing cells or actively through the nuclear pore complexes. The goal of this study was to investigate the relative importance of these two pathways for pDNA nuclear entry and subsequent gene expression.

Methods To measure nuclear entry of pDNA encoding enhanced green florescence protein (EGFP) in electrotransfected cells, we developed a sensitive technique for quantitative analysis of pDNA in the nuclei, based on a hybridization probe for pDNA detection at the single molecule level and automatic image analysis. In matched experiments, we used an mRNA targeted hybridization probe to quantify reporter mRNA expression per cell, and flow cytometry to quantify expression of EGFP.

Results We discovered two distinct patterns of pDNA distribution in the nuclei: punctate and diffuse, which were dominant in arrested and unarrested cells, respectively. The cell cycle arrest decreased diffuse pDNA and increased punctate pDNA. Its net effect was a decrease in the total intranuclear pDNA. Additionally, the cell cycle arrest increased the reporter mRNA synthesis but had no substantial impact on reporter protein expression.

Conclusion Results from the study demonstrated that the efficient nuclear entry of pDNA during cell division did not necessarily lead to a high level of transgene expression. They also suggested that the punctate pDNA was more transcriptionally active than diffuse pDNA in the nuclei. These data will be useful in future studies for understanding mechanisms of nonviral gene delivery.

Keywords Electrotransfection · Nonviral gene delivery · DNA nuclear entry

Introduction

Nonviral technologies have been widely used for delivery of plasmid DNA (pDNA) to cell nuclei for transgene expression [3, 9]. The delivery involves transport of pDNA across various physiological barriers. Among them, the nuclear envelope is a common barrier that has been limiting the efficiency of nonviral gene delivery in the past few decades [1]. Two mechanisms of pDNA nuclear entry are known in the literature although the details remain a target of investigation: passive inclusion during nuclear envelope breakdown (NEBD) and reformation in dividing cells, and active transport through nuclear pore complexes (NPCs) that is independent of cell division [7, 11, 19, 27].

Nuclear entry of non-virally electrotransfected DNA is generally considered more efficient in dividing cells than non-dividing ones. The consideration is supported by observations in previous studies. For example, transgene expression is often increased upon cell division [14, 22, 24], or when the nuclear envelope of electrotransfected cells is disassembled during or shortly after DNA electrotransfection [4, 5, 16, 31]. The cell division also leads to an increase in the intranuclear DNA [25]. While these studies suggest that cell division increases nuclear entry of DNA, the extent of this effect and the methodologies used to observe it vary greatly among different studies. The variation makes it difficult to come to a generalizable understanding of how important the cell division is for the nuclear entry of DNA and thus the success of nonviral DNA electrotransfection. To

Associate Editor Guohao Dai oversaw the review of this article.

✉ Fan Yuan
fyuan@duke.edu

[1] Department of Biomedical Engineering, Duke University, Durham, NC 27708, USA

address this uncertainty, we explored amplified hybridization probes for single DNA molecule detection and developed tools for automatic image analysis. They were used to characterize nuclear entry of pDNA post electrotransfection and its correlations to transcription and translation in dividing and non-dividing cells.

Materials and Methods

Cell Lines and Cell Culture

COS7, an African green monkey fibroblast-like kidney cell line, and HCT116, a human colorectal carcinoma cell line, and C2C12, a mouse myoblast cell line were obtained from the Duke University Cell Culture Facility (CCF). COS7 and C2C12 cells were cultured in DMEM (Gibco 11995-065) and HCT116 cells were cultured in McCoy's 5A medium (Gibco 16600-082). Both mediums were supplemented with 10% (v/v) bovine calf serum (Cytvia SH3007204) and 1% penicillin–streptomycin (Gibco 15140-122). Cells were incubated at 37 °C in 5% CO_2. Cells were passaged every 2–3 days and were not allowed to reach confluence.

Plasmids and Oligonucleotides

Plasmid pEGFP-N1 referred to as pEGFP was obtained from Nova Lifetech Inc. pMC.CMV-GFP-SV40PolyA was obtained from System Biosciences (SBI). pcDNA3.1(+)/Luc2=tdT, referred to as pLuc, was a gift from Christopher Contag (Addgene plasmid no. 32904). mCherry-LaminA-C-18 was a gift from Michael Davidson (Addgene plasmid no. 55068). All plasmids contained SV40, a DNA nuclear targeting sequence (DTS) that can facilitate pDNA nuclear entry [1]. Some pDNA samples were covalently labeled with Cy5 using the *Label* IT® kit (Mirus). The *Label* IT® reagent volume to DNA mass ratio was chosen to be 0.3 µL/µg, which led to one label for every 70–200 base pairs (Mirus). Primers for detection of pEGFP using qPCR were purchased from IDT, they are 5′-TGAACCGTCAGATCC GCTAG-3′ (forward) and 5′-GCTGAACTTGTGGCCGTT TA-3′ (reverse). We also validated a hybridization probe, Probe-EGFP-O4-Sense-C1 (ACD 1040801-C1), for pEGFP detection, and used another hybridization probe, Probe-EGFP-C2 (ACD 400281-C2), for detection of EGFP mRNA. Both probes were purchased from Advanced Cell Diagnostics (ACD).

Cell-Cycle Arrest

The cell-cycle was arrested by either thymidine or mimosine treatment. For thymidine mediated arrest, one million cells were plated and incubated for 24 h before treatment with thymidine (Sigma T1895). In the single-block of cell-cycle group, the treatment was at 2.5 mM for 18 h. In the double-block group, the cells were treated at 2 mM for 18 h, released in full medium for 8 h, and treated again for another 18 h. Following either procedure, the cell-cycle arrest was confirmed by flow cytometry analysis. To perform mimosine mediated arrest, approximately 2 million cells were plated in a 10-cm cell culture dish and incubated for 24 h upon which cells were 50–70% confluent. Cells were then treated with 400 µM L-mimosine (Sigma M0253) for 24 h. In all experiments, the untreated cells were prepared under the same conditions in parallel with the thymidine or mimosine treated cells.

Electrotransfection

Before transfection, the cells were detached from culture plates using 0.25% trypsin (Gibco 1505-057), split into aliquots of 1×10^6 cells, and washed with DPBS (Gibco 14190-144). For each electrotransfection, 1×10^6 cells were resuspended in 100 µL of pulsing buffer, consisting of 2 µg pDNA in OptiMEM reduced serum medium + GlutaMAX (Gibco 51985-034), and transferred to a 4 mm gap electroporation cuvette (Genesee 40-102). An electric pulse sequence was applied to cells (2 pulses at 150 V for COS7 and HCT116 cells, 250 V for C2C12 cells, 10 ms duration, and 0.1 Hz frequency) using an ECM 830 square wave electroporation system (BTX). Cells were then immediately mixed with the full medium (1 mL) that had been prewarmed to 37 °C, and seeded in either 6-well plates or #1.5 glass bottom dishes (Cellvis D35-20-1.5-N). In some groups, the full medium was supplemented with thymidine or mimosine at the same concentration as that used in the cell cycle arrest protocol. All cells were incubated for 16 or 24 h prior to fluorescence microscopy and flow cytometry analyses. The pulsing conditions described above were also used to deliver two plasmids into COS7 cells. Briefly, 5 million cells were first pulsed with 12.5 µg of a plasmid encoding mCherry-LaminA-C-18, and incubated for 7 h before being replaced in the DMEM with 400 µM mimosine. The cells were then incubated for 24 h, electrotransfected with Cy5-pEGFP. After 16 h, samples were washed with DPBS, fixed with 3% PFA in DPBS for 15 min at room temperature, and stained with 10 µg/µL Hoechst (Thermo Fisher Scientific H1399) for 10 min at room temperature. The samples were protected from light prior to microcopy analysis.

In Situ Hybridization with RNA and DNA Probes

The hybridization was performed in cells electrotransfected with unlabeled pEGFP. Cultured cell samples were washed with DPBS, fixed with 4% PFA in DPBS, then prepared according to the RNAscope Multiplex Fluorescent Reagent

Kit v2 user manual (ACD) with some modifications. All reagents were supplied in the RNAscope Multiplex Fluorescent Reagent Kit v2 (ACD 323100) unless otherwise stated. Fixed cell samples were first incubated with hydrogen peroxide for 10 min at room temperature, then washed with ultrapure distilled water (Invitrogen 10977-015).

To analyze pEGFP in cells, the samples were incubated with RNA digestion buffer (25 µg/mL RNase A in 1 × Tris-buffered saline with 0.05% TWEEN 20) (Sigma P2287) for 30 min at 37 °C then washed twice with DPBS [10]. Then, the samples were treated with protease III for 10 min at room temperature before washing twice with DPBS. Samples were incubated in prewarmed DNA denaturation buffer [75% formamide (Roche 11814320001) in 2 × SSC (Invitrogen 15557-044)] for 5 min at 75 °C to increase hybridization efficiency [32], washed once with DPBS, then incubated with Probe-EGFP-O4-Sense-C1 for 4 h at 40 °C. To analyze EGFP mRNA in cells, the samples were incubated with Probe-EGFP-C2 for 2 h at 40 °C. After probe hybridization in both cases, the samples were washed twice with RNAscope wash buffer, incubated in 5 × SSC overnight at 4 °C. All samples were then incubated with two hybridization probe amplifiers successively for 30 min, then with a third amplifier for 15 min, all at 40 °C, washing with RNAscope wash buffer between incubations. After amplification, probe fluorescence signal was developed by incubating first with HRP for 15 min, then with Opal 690 (Akoya FP1497001KT) diluted 1:1500 in TSA buffer for 30 min both at 40 °C, washing with the RNAscope wash buffer after each incubation. Samples were then stained with 10 µg/µL Hoechst for 10 min at room temperature, protected from light prior to microcopy analysis.

Fluorescence Microscopy and Image Analysis

Fluorescence images for mRNA and pDNA analyses were taken using an Andor Dragonfly spinning disk confocal plus microscope equipped with a × 63 oil objective and a 40 µm pinhole disk or with an Axio Observer microscope equipped with a × 40 air objective for widefield images. The super-resolution radial fluctuations (SRRF) algorithm as implemented in Andor's Fusion software was used to acquire super-resolution images with 120–150 nm spatial resolution. Two channel images were acquired for all samples, one for Hoechst stained nuclei (405 nm laser, 10 ms excitation, 10% power, 450/50 nm emission filter) and the other for pDNA or mRNA labeled with either Cy5 or Opal690 (637 nm laser, 10 ms excitation, 7% power, 700/75 nm emission filter). All images were optical slices; and each of them was chosen to be near the central plane of most cell nuclei in the field of view. Out of focus nuclei were excluded automatically or manually based on the Hoechst signal.

Image analysis was performed with CellProfiler. For automatic analysis, we developed a procedure to quantify intranuclear pDNA outlined in Fig. 1a. Nuclei were identified as objects in the Hoechst channel 150–600 pixels (~7–29 µm) in diameter after thresholding with the robust background method and smoothing to avoid objects with excessively jagged edges. The size range was set empirically, based on the lowest and highest diameters of the nuclei observed in a small subset of images. Out-of-focus nuclei were then filtered out based on form factor, defined as $4\pi(area)/perimeter^2$. In-focus nuclei had a distinct Hoechst outline resulting in an object with smooth perimeter and a form factor between 0.7 and 1, whereas out-of-focus nuclei had a more jagged perimeter resulting in a form factor less than 0.6. To exclude out-of-focus nuclei automatically, nucleus objects with a form factor less than 0.6 were discarded. In-focus nuclei were then split into an edge region and inner region. To do so, nuclei were split into eight concentric rings, scaled based on the object size, and the outermost ring was considered the nuclear edge while the combined area of the remaining rings were considered the inner nucleus (see Fig. 1b). In parallel to nucleus segmentation, pDNA images in far red channel were processed. First, background of these images was subtracted based on measured intensity of negative control images (samples electrotransfected with no plasmid or with pLuc, a plasmid not recognized by the hybridization probe) captured with the same parameters in far red channel. Then, pDNA punctates were detected as objects 4–40 pixels (190–1900 nm) in diameter with intensity greater than a manually set threshold. The size range was determined empirically, based on measurements of visually distinguished punctates, and the threshold was set by trial-and-error to distinguish punctate DNA from surrounding diffuse DNA in a small subset of images (see Fig. 1b). The outputs were the integrated fluorescence intensities of punctate and diffuse signals of pDNA per nuclear section, respectively, as well as the number of punctates per nuclear section.

The process used to quantify mRNA is outlined in Fig. 1c. Nuclei were detected as in pDNA quantification, then nuclear objects were expanded until touching to create a mosaic in which each region corresponds to a single cell (see Fig. 1d). In parallel, mRNA images were background subtracted, then integrated fluorescence intensity of mRNA signal per cell region was measured.

Widefield fluorescence microscopy was used to image samples prepared with the Click-iT RNA Alexa Fluor 594 Imaging kit (Invitrogen C10330) and automated image analysis was used to quantify total RNA signal per cell. These images were quantified in the same way as images for mRNA quantification—nuclei were segmented and expanded to identify cell regions, then total RNA was quantified as integrated fluorescence intensity per region.

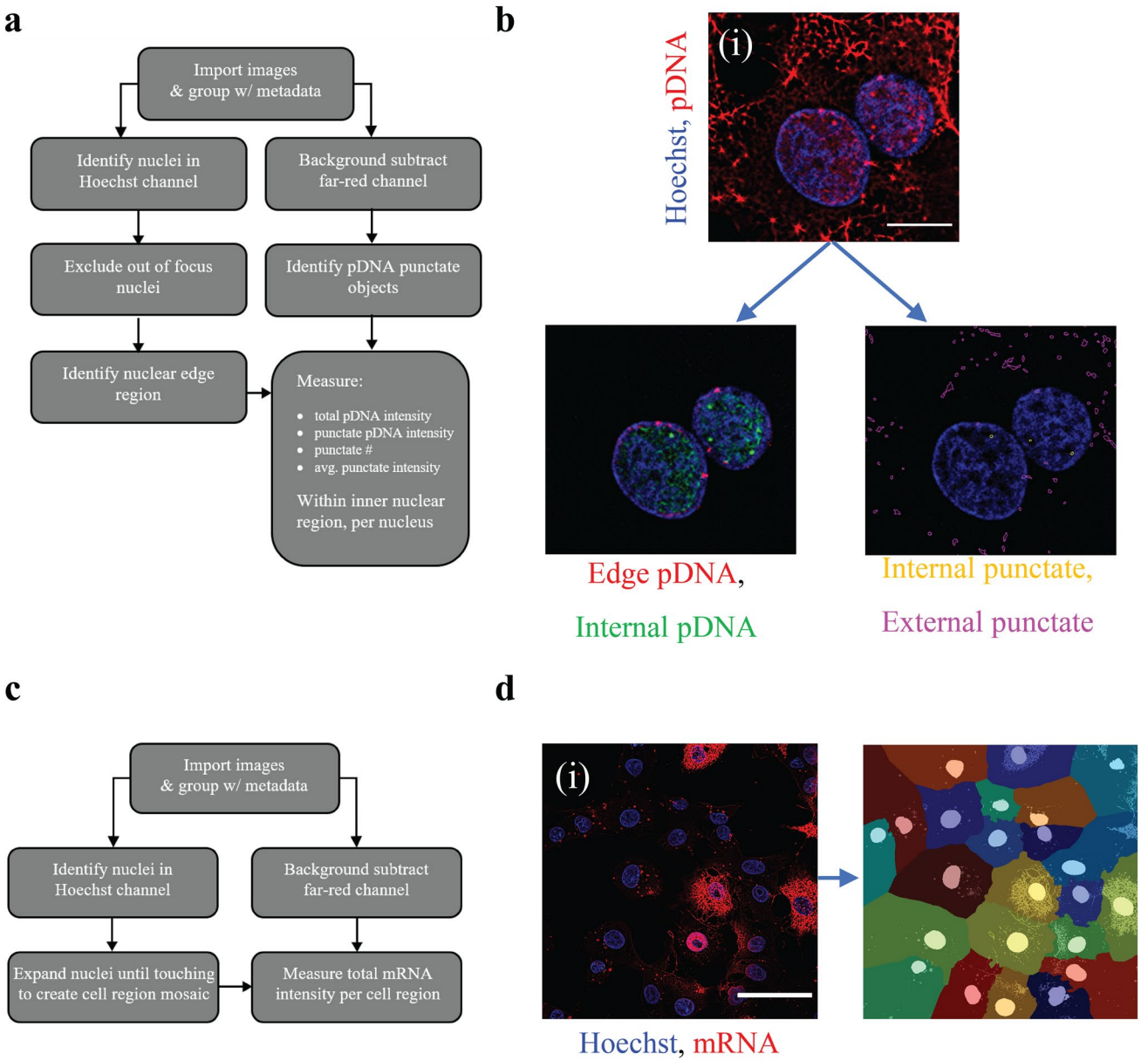

Fig. 1 Super-resolution confocal imaging and image analysis for pDNA nuclear entry and reporter mRNA expression. It shows the procedures used for quantification of nuclear pDNA signals (**a**, **b**), and reporter mRNA per cell (**c**, **d**). **a** Flow chart for image analysis for pDNA quantification. **b** Illustration of imaging experiment for nuclear pDNA quantification in three steps. (i) Image acquisition. Nuclei and pEGFP in fixed cells were labeled with Hoechst dye (blue) and the DNA hybridization probe (red), respectively. The image was acquired with super resolution confocal microscopy. Scale bar 10 μm. (ii) Image segmentation. Using CellProfiler, nuclei were segmented and the area within each nucleus was divided into two regions: internal and edge. pDNA on the edge (red) must be excluded because it was uncertain whether the pDNA was beyond the nuclear envelope. Only the internal pDNA (green) was considered in the nuclear entry analysis. (iii) Mask generation for punctate pDNA. Two patterns of inner pDNA distribution were observed: punctate and diffuse. Individual punctates were identified based on signal intensity level and size of pixel clusters. These objects were then used to generate masks for internal punctate (yellow) and edge or external punctate (magenta) to separate the total pDNA signals within the nucleus into punctate and diffuse signals. After background subtraction, fluorescence intensities of different pDNA signals and number of punctates were quantified separately in individual nuclei. **c** Flow chart for image analysis for mRNA quantification. **d** Illustration of imaging experiment for reporter mRNA quantification. (i) Image acquisition. Nuclei and EGFP mRNA in fixed cells were labeled with Hoechst dye (blue) and the RNA hybridization probe (red), respectively. The image was acquired with super resolution confocal microscopy. Scale bar 50 μm. (ii) Using CellProfiler, the nuclei were segmented then expanded until borders of all nucleus-derived objects were in contact. This split the image into a mosaic in which each region contained only one nucleus. After background subtraction, integrated fluorescence intensity of mRNA signals in each region was used as an estimation for the amount of EGFP mRNA per cell

Flow Cytometry

For transgene expression and cell density analyses, pEGFP electrotransfected cells and matched controls were washed with DPBS and collected at 24 h post electrotransfection, resuspended in 1 to 1.2 mL DMEM, and acquired for flow cytometry analysis (NovoCyte 1050 flow cytometer and the companion software NovoExpress). 30,000 Single cells were run for each sample. Single cell gates were set using untransfected control samples based on forward and side scattered light. EGFP signal was detected at 488 nm excitation and the gate for distinguishing EGFP positive cells was set using untransfected control samples. Transgene expression was evaluated with two metrics: electrotransfection efficiency, defined as the percent of viable cells positive for EGFP signal, and expression level, defined as the geometric mean of EGFP intensity in the positive population. The cell density in each sample was calculated as the number of cells per unit volume of cell suspension.

For analysis of cell proliferation, mimosine treated or untreated cells were electrotransfected with pLuc (a plasmid without fluorescent transgene products to avoid interference with the assay readout), then incubated in the full mediums supplemented with 2 mM EdU for 16 h. For cells in the treated groups, the mediums were also supplemented with mimosine (400 µM) to maintain the state of cell-cycle arrest. At the end of the incubation, the cells were stained with a fluorescent marker using Click-iT Plus EdU Alexa Fluor 488 Flow Cytometry Assay Kit according to manufacturer's instructions (Invitrogen C10632). Briefly, cells were fixed and permeabilized with the reagents included in the kit, washed intermittently with 1% BSA in PBS. A click reaction was then performed to attach Alexa Fluor 488 to EdU incorporated by cells during the 16-h incubation, followed by subsequent washing with the provided permeabilization and wash reagent before flow cytometry analysis. EdU was detected at 488 nm excitation and the gates for distinguishing single cells and EdU negative cells were established on matched control samples that were incubated without EdU. Gates for stages of proliferation were set based on two apparent peaks and the space between them (see Fig. 2). The lower intensity peak aligned with no EdU control samples and corresponds to the cell-cycle arrested cells with no EdU incorporation, while the higher intensity peak represents cells that had undergone at least one full S phase and incorporated the most EdU, classified as late S phase/divided cells. The space between the two peaks with ascending EdU intensity corresponds to early/mid S phase. The analysis above could not be performed after cell-cycle arrest with the thymidine treatment, because of the similarities in chemical structures between thymidine and EdU. Since we could not verify the percent of non-dividing cells in thymidine treated group, mimosine treatment was mainly used to block cell division in the current study.

Total RNA Synthesis and Total Protein Level Measurement

For quantification of total RNA synthesis in untransfected cells, samples were prepared with the Click-iT RNA Alexa Fluor 594 Imaging kit (Invitrogen C10330) according to manufacturer's instructions. Briefly, cell

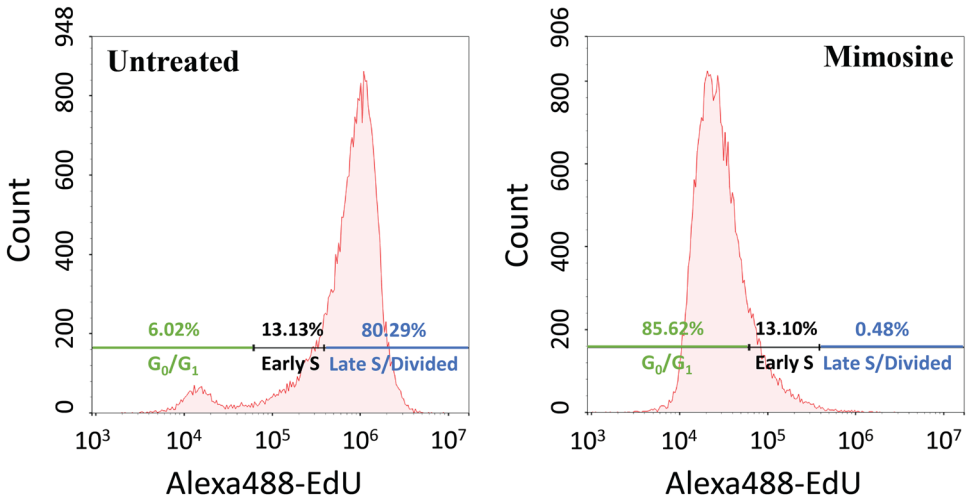

Fig. 2 Quantification of cell proliferation with EdU. COS7 cells were plated and pretreated with mimosine for 24 h or untreated (control), followed by electrotransfection of pLuc and incubation with EdU for 16 h. The medium was supplemented with mimosine for the pretreated group or nothing for the untreated group. At the end of the incubation, the cells were analyzed with flow cytometry. The histograms of EdU signal were used to quantify the percentages of cells in G0/G1 phase, early S phase, and late S phase/fully divided, respectively, during the 16-h incubation

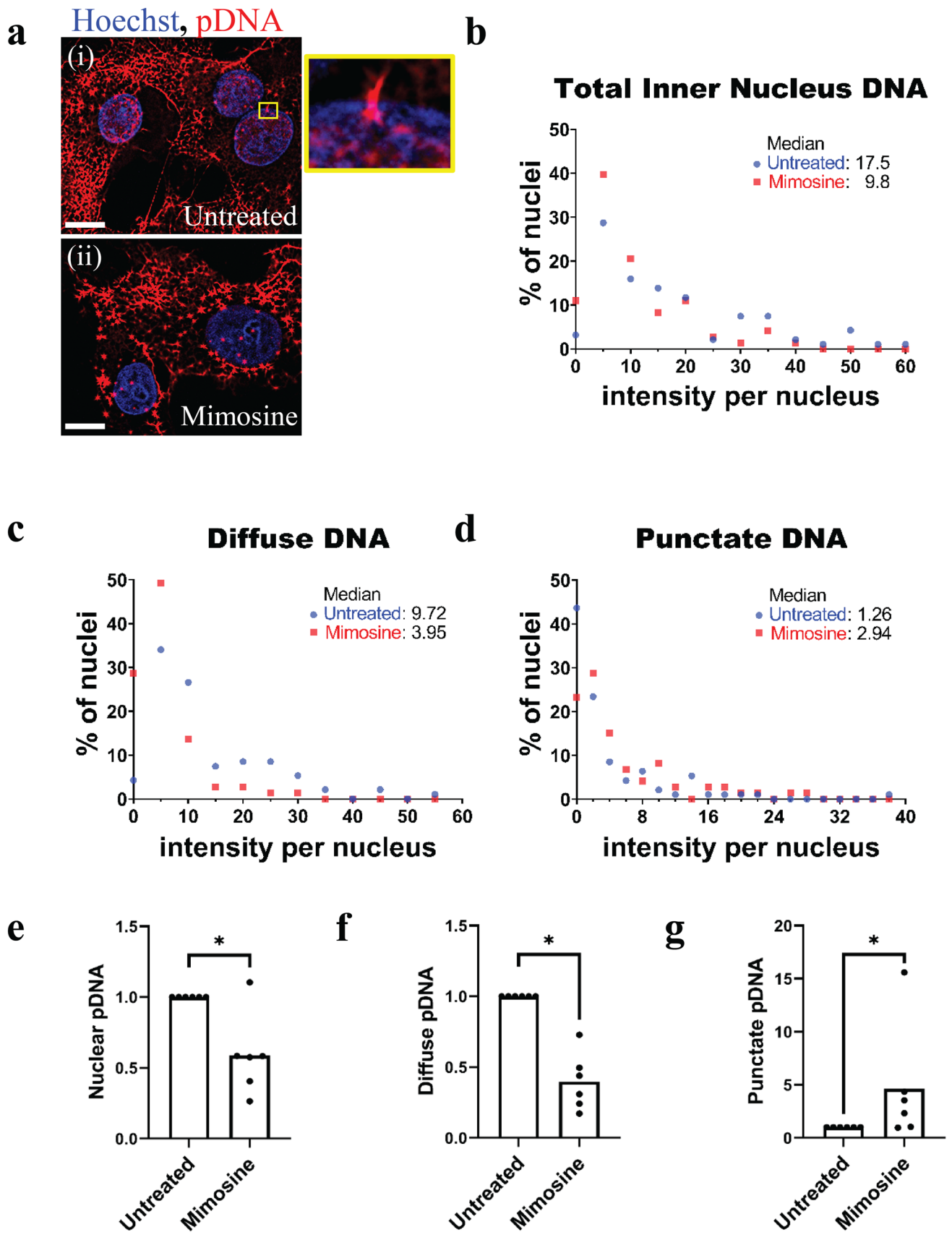
a
Hoechst, pDNA
(i)
Untreated
(ii)
Mimosine
b
Total Inner Nucleus DNA
Median
Untreated: 17.5
Mimosine: 9.8
% of nuclei
intensity per nucleus
c
Diffuse DNA
Median
Untreated: 9.72
Mimosine: 3.95
% of nuclei
intensity per nucleus
d
Punctate DNA
Median
Untreated: 1.26
Mimosine: 2.94
% of nuclei
intensity per nucleus
e
Nuclear pDNA
Untreated
Mimosine
f
Diffuse pDNA
Untreated
Mimosine
g
Punctate pDNA
Untreated
Mimosine

◂**Fig. 3** Quantitative analysis of DNA nuclear entry in cell-cycle arrested and unarrested cells. COS7 cells pretreated with mimosine for 24 h and untreated controls were electrotransfected with pEGFP followed by incubation for 16 h in the full medium with and without continued mimosine treatment, respectively. Thereafter, the cells were fixed and stained with the Hoechst dye (blue) for nuclei and the DNA probe (red) for pEGFP. Images at the central plane of > 25 nuclei were acquired with confocal microscopy in each group, with a total of 245 nuclei for the treated cells and 443 nuclei for the untreated cells across 6 independent repeats. **a** Typical super-resolution images of pDNA distributions in (i) untreated cells, and (ii) mimosine treated cells. Scale bars 10 μm. The magnified region in (i) shows an elongated pDNA molecule across the nuclear envelope. **b**–**d** Distributions of fluorescence intensity per nucleus for pEGFP signals in mimosine treated and untreated cells quantified in a typical experiment (n > 25). Bin widths are 5 au in **b**, **c**, and 2 au in **d**. **e**–**g** Medians from the histograms normalized by the data from the untreated cells in six independent repeats. The intensities were quantified separately for total pEGFP signal (**b**, **e**), diffuse signal (**c**, **f**), and punctate signal (**d**, **g**), respectively. *P < 0.05; n = 6; Mann–Whitney U test

cycle arrested and unarrested cells were incubated with 0.2 mM 5-ethynyl uridine (EU) solution for 16 h, and the solution was supplemented with 400 μM mimosine in the cell cycle arrested group. Cells were then fixed with 10% formalin, permeabilized with 0.5% Triton X-100, and incubated with the reaction cocktail prescribed to attach Alexa Fluor 594 to EU incorporated into RNA during the 16-h synthesis. Before imaging, the nuclei of cells were stained with 10 μg/μL Hoechst for 10 min at room temperature. Cells incubated with no EU were used as a negative control.

To measure the total protein content, cells were cultured for 48 h with or without treatment with 400 μM mimosine, then trypsinized, counted, and aliquoted such that each experimental group had an identical number of cells. Cells were pelleted by centrifuging at 280 × g for 5 min and then re-suspended in 250 μL lysis buffer—1% (v/v) Triton X-100, 50 mM Tris, pH 7.5, 750 mM NaCl, 5 mM EDTA, with 1:100 diluted protease inhibitor cocktail (Sigma-Aldrich P8340) added just before using. Cells were incubated on ice for 5 min and at room temperature for 10 min, vortexing every 5 min. Lysed cells were then centrifuged at 17,000 × g for 30 min. Lysate supernatant was collected and the Pierce BCA Protein Assay Kit (Thermo Scientific 23227) was used according to manufacturer's instructions to quantify total protein per cell. Briefly, 25 μL of each standard (working range = 20–2000 μg/mL) or experimental sample was pipetted into wells of a 96 well plate, followed by the addition of 200 μL working reagent and incubation at 37°C for 30 min. A plate reader was then used to measure the absorbance of all samples at 562 nm. A standard curve was prepared and used to convert blank subtracted absorbance readings to protein concentrations (μg per million cells).

Statistical Analysis

Statistical analysis was performed with GraphPad Prism software. Mann–Whitney U test was used to determine the significance of differences between two experimental groups, and the Kolmogorov–Smirnov test was used to determine the significance of differences between two histograms. For all statistical analyses, a difference was considered to be statistically significant if $P < 0.05$. In data from imaging experiments, we noted the presence of outliers in terms of total intranuclear fluorescence intensity and pDNA punctate numbers. These outliers were likely to be caused by signals from dead cell contaminations even after sample washing. The outliers were identified using the ROUT method as previously described [26], with Q = 1%, and excluded from data analysis.

Results

Nuclear Entry of pDNA in Cell-Cycle Arrested and Unarrested Cells

COS7 cells were equally divided into two groups. The cell-cycle was unarrested in one group, and arrested in another group by treatment with mimosine. Then, the cells were electrotransfected with pEGFP and incubated for 16 h before being fixed and stained with a DNA hybridization probe for pEGFP. After amplification of the probe signal, the level of intranuclear pEGFP was quantified with super-resolution confocal microscopy and image analysis. We observed that the arrested cells were larger than untreated ones, which was consistent with previous observations where the cell cycle is arrested with other chemicals [5]. The pEGFP signal distributed within the cell nuclei with a broad range of intensity, and two distinct patterns: diffuse and punctate. The diffuse signal spread homogeneously throughout the nucleus; and the punctate signal was discontinuous and had diameters of 190–1900 nm (Fig. 3a). Additionally, the DNA punctates were brighter than diffuse DNA, allowing the patterns to be quantified separately in automated image analysis (see Fig. 1b). Interestingly, we also captured the nuclear entry process of pEGFP in some images, where DNA molecules were elongated when passing the nuclear envelope, presumably through the nuclear pore complexes (Fig. 3a).

The cell-cycle arrested cells tended to have more punctate, less diffuse, and lower overall signal intensity per nucleus compared with the unarrested cells (Fig. 3b–d). The difference in the histogram of each signal type between arrested and unarrested cells was statistically significant in five out of six independent repeats ($P < 0.05$, Kolmogorov–Smirnov test) (data not shown). For each paired-experiment, we also quantified the median fluorescence intensity

among the cell-cycle arrested cells, and normalized it by that among the unarrested cells. The means of the normalized data from six independent repeats were 0.56 for total pEGFP signal, 0.42 for diffuse signal, and 3.58 for punctate signal (Fig. 3e–g); the differences were statistically significant ($P < 0.05$). Since the signal intensity was correlated to the amount of pEGFP per nucleus, the data above indicated that the cell-cycle arrested cells had more punctate pEGFP, less diffuse pEGFP, and lower amount of total pEGFP per nucleus, compared to the unarrested ones.

To determine if the formation of two distinct pDNA patterns was a universal phenomenon, we repeated the same experiment as above using HCT116 and C2C12 cells. Indeed, both diffuse and punctate patterns of pEGFP were observed in these cell types (Fig. 4). To validate the observations of pEGFP in the nucleus based on quantitative image analysis, we performed two negative control experiments following the same procedures as above, except that the cells were either electrotransfected with pLuc—a plasmid that could not be hybridized with the DNA probe—or untransfected with plasmids. Typical images of cells in control and experimental groups are shown in Fig. 5. In pLuc electrotransfected cells, no diffuse fluorescence was observed after staining with the DNA probe. Additionally, we observed that 84% of the nuclei had no fluorescence punctates, 15% of them had a single punctate, and 1% of them had two punctates. The data indicated that a majority of the control nuclei did not show signals from the DNA probe. In untransfected

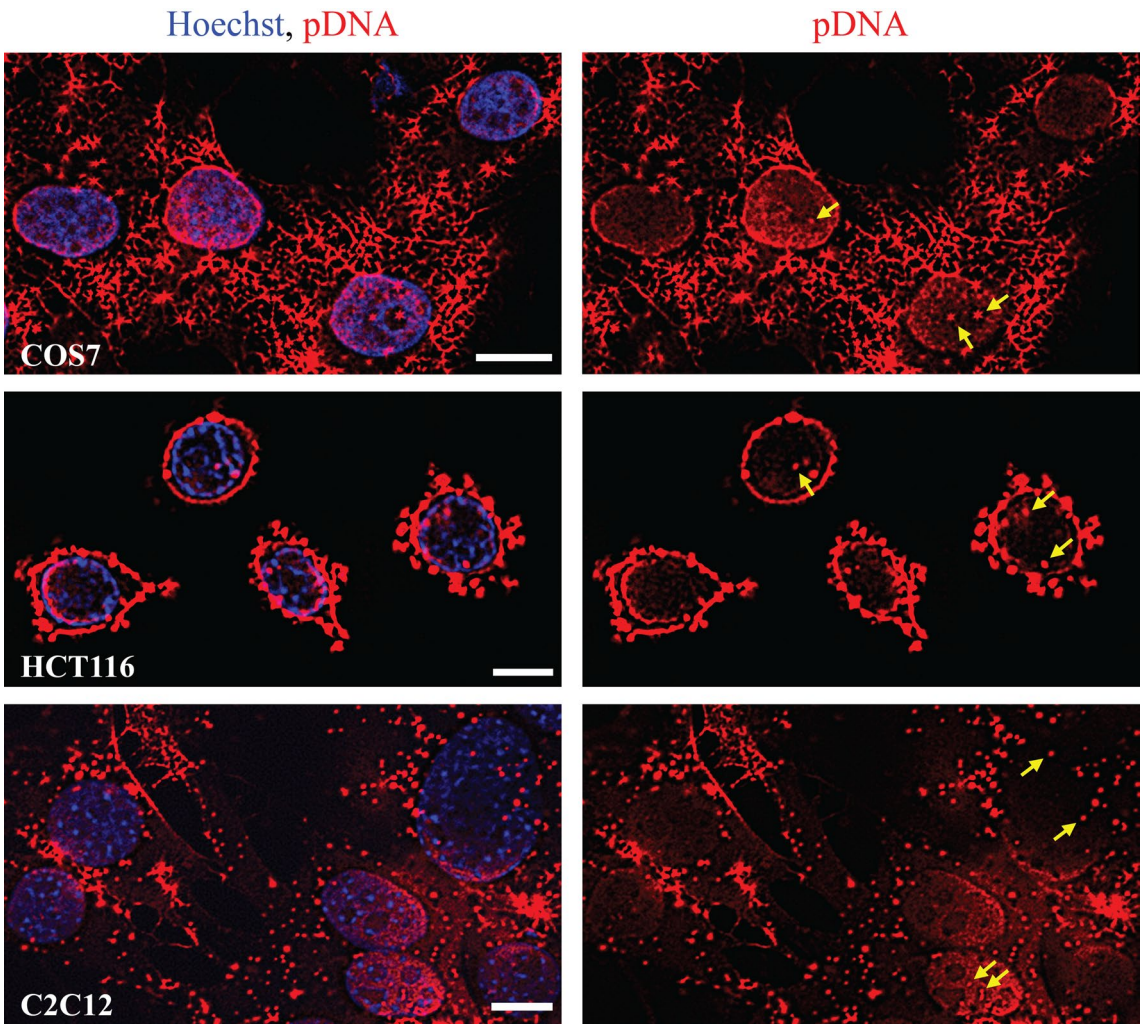

Fig. 4 Diffuse and punctate DNA patterns in different cell types. Untreated cells were electrotransfected with pEGFP followed by incubation for 16 h in the full medium. Thereafter, the cells were fixed and stained with the Hoechst dye (blue) for nuclei and the DNA hybridization probe (red) for pEGFP. The images show the optical sections near the central plane of nuclei in confocal microscopy for different samples. In the left column, Hoechst and the DNA probe signals are overlaid, and in the right column, the same regions of cells with the signal from DNA probe only are shown to emphasize DNA distribution patterns. Some punctate examples are indicated with yellow arrows. The images from COS7, HCT116, and C2C12 cells are shown in the top, the middle, and the bottom rows, respectively. Scale bars 10 μm

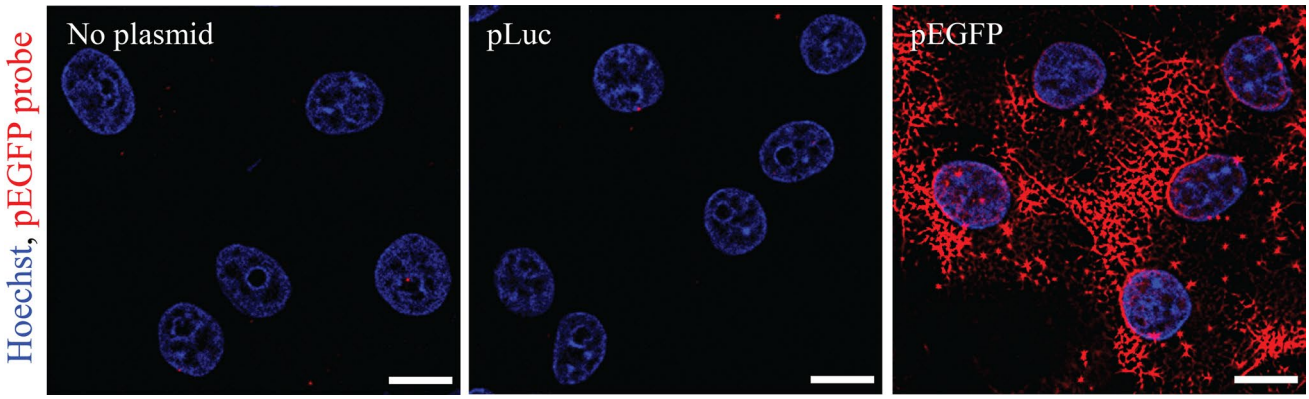

Fig. 5 DNA probe signal in negative controls. Untreated COS7 cells were electrotransfected with no plasmid (left), pLuc (middle), or pEGFP (right) then cultured for 16 h in full medium. Cells were then fixed and stained with Hoechst and a DNA hybridization probe for pEGFP. Images show the optical sections near the central plane of nuclei in confocal microscopy for different samples. Scale bar 10 μm

cells, similar results were observed (data not shown). The punctate signal in the control groups might be caused by non-specific binding of the probe to nuclear structures that could not be washed away after cell staining. In addition to the punctate number measurement, we set the maximum fluorescence intensity in the control nuclei without punctates as the background threshold, and compared it with data in different experimental groups. We observed that the fluorescence intensity per nucleus was higher than the threshold in > 99% of pEGFP electrotransfected cells. Together, the data above indicated that the nuclear entry of pEGFP occurred in the majority of the cells post electrotransfection, independent of the cell-cycle arrest.

Next, we determined if the release of cells from the cell-cycle arrest could affect the nuclear entry of pDNA. The experimental design was similar to the experiments described above. The only difference was that the cells were not treated with mimosine post electrotransfection in one of the groups, releasing the cell-cycle arrest. We observed that the median intensity of total DNA signal per nucleus was higher in the released group than the unreleased one, mainly due to the increase in the diffuse signal. Quantitatively, the median intensities of diffuse and punctate DNA signals in the released cells were 3.4 times and 3.1 times as high as those of the unreleased cells, respectively, in one experiment; or 2.3 and 1.0, respectively, in an independent repeat (Fig. 6). The data suggest that the inhibitory effect of the mimosine treatment on DNA nuclear entry is reversible.

To better understand the data discussed above, we also quantified the total amount of cells divided over a period of 16 h post electrotransfection of pLuc using the EdU assay. Our data showed that 85.6% of the mimosine treated cells were arrested in the G_0/G_1 phase, and less than 1% of them reached the late S phase or fully divided (Fig. 2), indicating that the NEBD occurred only in a tiny fraction of the mimosine treated cells. In the untreated group, at least 80% of the cells reached the late S phase or fully divided in the 16-h period.

The intranuclear signals of pDNA discussed above were investigated after the cells were fixed and stained with the DNA probe. We also performed the nuclear entry experiments using Cy5 labeled pDNA (Cy5-pDNA), a commonly employed technique for visualization of pDNA in both live and fixed cells. We electrotransfected COS7 cells with Cy5-pEGFP in both mimosine treated and untreated cells, and compared Cy5 signals in the nuclei at 16 h post electrotransfection, using the same methods as those described above for the DNA probe detection and analysis. The Cy5 signals could be observed as single or small clusters (i.e., punctates) of pixels. Most punctates were less than 480 nm in size and with a small range of fluorescence intensity (Fig. 7), which differed from the fluorescence signals from the DNA probes (Fig. 3a). Thus, we chose to quantify the pDNA signal as the total number of Cy5 positive pixels instead of Cy5 fluorescence intensity per nucleus. The median number of Cy5-pDNA positive pixels per nucleus in mimosine treated cells was 1.49 times as high as that in untreated controls (Table 1). The observation was qualitatively consistent with the punctate signals of the DNA probe for pDNA without Cy5 label (Fig. 3g). However, the diffuse signal of Cy5-pDNA was rarely observed in both mimosine treated and untreated groups. The observations were similar when the study was repeated with different pDNA and cell preparations: (a) electrotransfection of Cy5 labeled pMC.CMV-GFP-SV40PolyA into COS7 cells untreated or treated with mimosine or thymidine (the treatment led to cell-cycle arrest at G_1/S) [5], and (b) electrotransfection of Cy5 labeled pEGFP into mimosine treated or untreated HCT116 cells (see Table 1). These observations demonstrated that only the punctate signals from Cy5-pDNA could be detected under a fluorescence microscope (see Fig. 7); the fluorescence signals of the diffuse

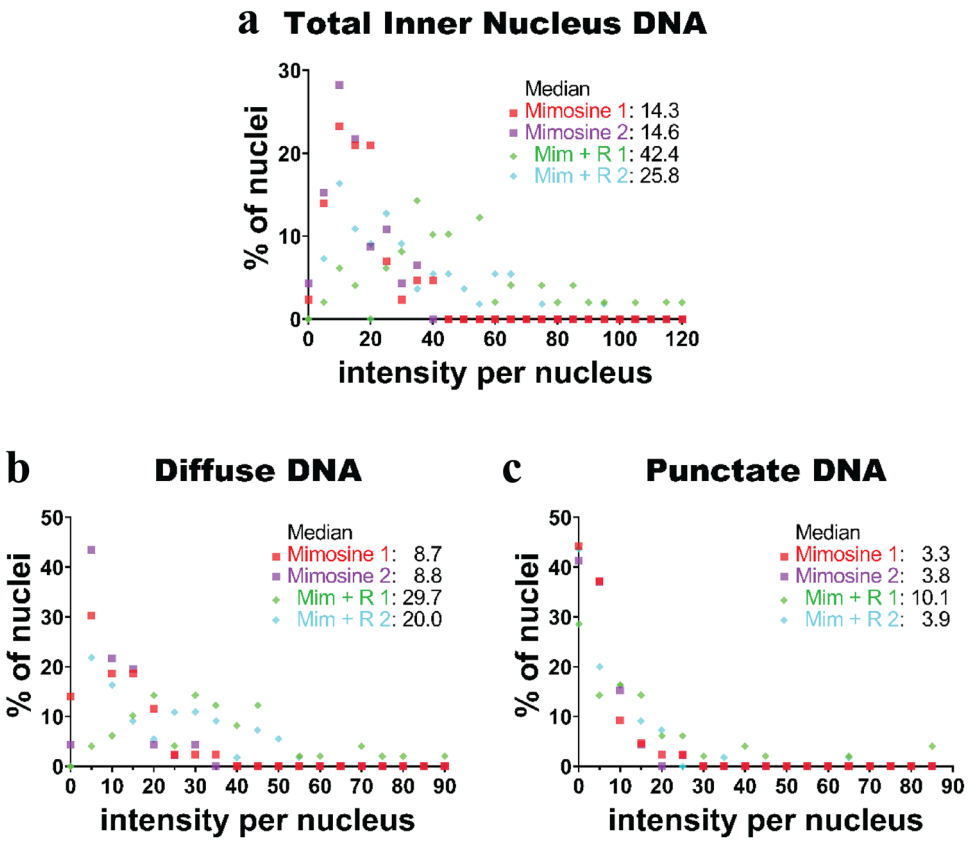

Fig. 6 Effects of release from cell-cycle arrest on nuclear entry of pDNA. COS7 cells were pretreated with mimosine for 24 h, followed by electrotransfection of pEGFP and incubation for another 16 h. The incubation medium was supplemented with mimosine in the continued arrest group (Mimosine) or nothing to release the cells from the cell-cycle arrest (Mim + R). At the end of incubation, the cells were fixed and stained with Hoechst dye for nuclei and DNA probe for pEGFP. The histograms for pEGFP signal intensity per nucleus were obtained with confocal microscopy and image analysis. The panels show the data from two independent repeats. **a** Total pEGFP signals, **b** diffuse signals, and **c** punctate signals. The bin widths in all plots are 5 au. The differences between the two groups (Mimosine vs. Mim + R) were significant for the total and diffuse signals in both experimental repeats ($P < 0.05$), but the P value was < 0.05 only in one of the repeats for the punctate signals (Kolmogorov–Smirnov test, $n > 40$ per group in each repeat)

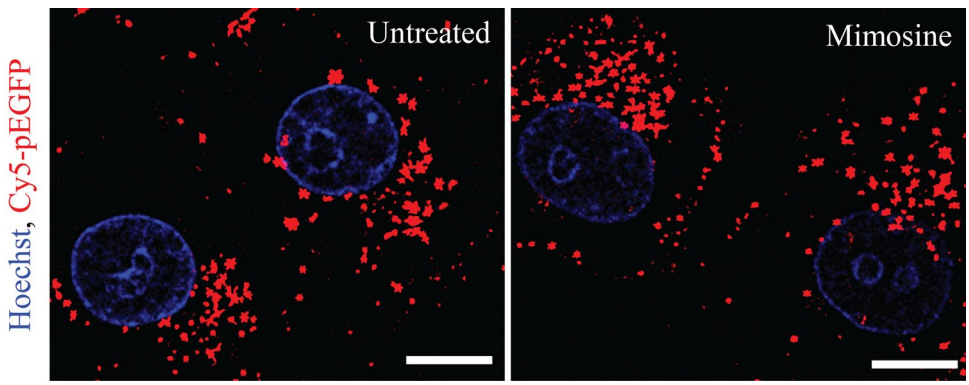

Fig. 7 Typical super-resolution images of Cy5-pEGFP in cells. COS7 cells were treated with mimosine (400 μM, 24 h) or untreated, followed by electrotransfection of Cy5-pEGFP. Then, cells in the two groups were incubated for 16 h in the medium supplemented with mimosine (400 μM) and nothing (untreated), respectively. Cy5-pEGFP signals in cell nuclei were visible under the super-resolution microscope as single isolated pixels or small clusters of pixels (less than 10)

Table 1 Ratios of Cy5-pDNA positive pixel numbers between cell-cycle arrested and unarrested cells

Treatment	Cell type	Plasmid	Pixel number ratio
Mimosine	COS7	pEGFP	1.49
Mimosine	HCT116	pEGFP	4.44
Mimosine	COS7	pMC	1.04
Thymidine	COS7	pMC	1.74

Each cell type was divided into two groups. Cell-cycle was arrested in the first group with either thymidine or mimosine treatment for 24 h, and unarrested in the second group. Cells in both groups were electrotransfected with Cy5 labeled pEGFP or pMC.CMV-GFP-SV40PolyA (pMC) and incubated for 16 h. The medium was supplemented with thymidine or mimosine in the first group and nothing in the second group. At the end of incubation, the number of Cy5 positive pixels per nucleus was quantified in all cells. For each pair of groups, the ratio of the median numbers between cell-cycle arrested and unarrested cells was calculated

Cy5-pDNA were likely to be too weak to be detected with the method used in our study.

Our next experiment was to determine if punctate pDNA detected in cell nuclei was truly within the cell nucleus. We used COS7 cells overexpressing mCherry-Lamin-A-C-18 in the electrotransfection experiment, allowing us to visualize the inner boundary of each nucleus. We found that a majority of Cy5-pDNA detected near the central plane of cell nuclei in all confocal images were not associated with invaginations or wrinkles of the nuclear envelope [13] (see Fig. 8). On the other hand, co-localization of Cy5-pDNA with the inner boundary of nuclei was observed more commonly on the smooth edge of the nuclei than in the nuclear envelope invaginations, and in many instances, the Cy5-pDNA appeared elongated through the nuclear envelope. All signals at the edge were excluded in our image analysis. Therefore, the data reported in Table 1 were numbers of pixels with intranuclear Cy5-pDNA.

Transgene Expression in Cell-Cycle Arrested and Unarrested Cells

The mRNA level per cell was quantified to evaluate effects of the mimosine treatment on transcription of EGFP using an imaging approach similar to that for intranuclear pDNA quantification (see Fig. 1d). Specifically, COS7 cells in one group were treated with mimosine for 24 h prior to electrotransfection of unlabeled pEGFP, and 16 h post electrotransfection. The cells in the other group were untreated controls. All cells were stained with a hybridization probe for the mRNA and examined under a confocal microscope (Fig. 9a). Distributions of mRNA intensity per cell within a typical sample are shown in Fig. 9b. The distributions in all three experimental repeats were significantly different between untreated and mimosine treated samples ($P < 0.05$, Kolmogorov–Smirnov test) (data not shown). The medians of mRNA signal intensity per cell in the cell-cycle arrested samples were 2.1–6.5 times as high as the unarrested ones in three independent repeats (Fig. 9b, c). Considering the lower amount of intranuclear pEGFP observed in the cell-cycle arrested cells, the mRNA data suggest that the rate of EGFP transcription is higher in

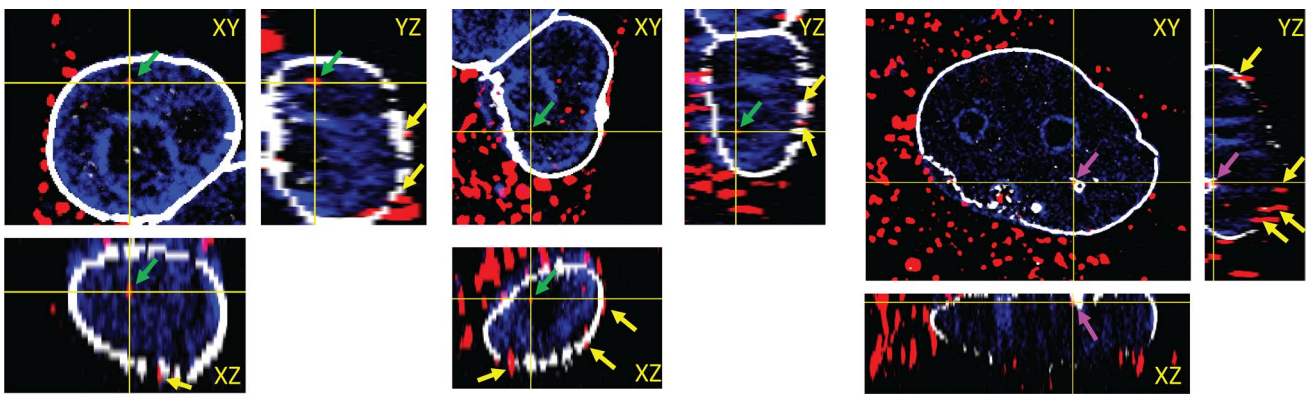

Fig. 8 Visualization of punctate pDNA and nuclear envelope. COS7 cells overexpressing mCherry LaminA-C-18 (white) were treated with mimosine (400 μM, 24 h), followed by electrotransfection of Cy5 labeled pEGFP (red). Then, the cells were incubated for 16 h in the medium supplemented with mimosine (400 μM) to increase the number of pDNA punctates. At the end of incubation, the cells were fixed, nuclei were stained with Hoechst (blue), and imaged with a super-resolution confocal microscope. Z-stacks were captured with a 0.5 μm step size that spanned cell nuclei to determine if Cy5-pEGFP punctates overlapped with nuclear envelope in the invaginations and on the smooth surface. For each nucleus shown above, a central slice is shown in the XY plane and orthogonal views are shown in the YZ and XZ planes. Green arrows point to Cy5-pEGFP punctates in the central plane that are not connected to any Lamin structure, indicating that they are within the nucleus. Magenta arrows point to Cy5-pEGFP punctates in the central plane that are within nuclear envelope invaginations. Yellow arrows point to Cy5-pEGFP punctates that are in contact with or across the smooth surface of the nuclear envelope

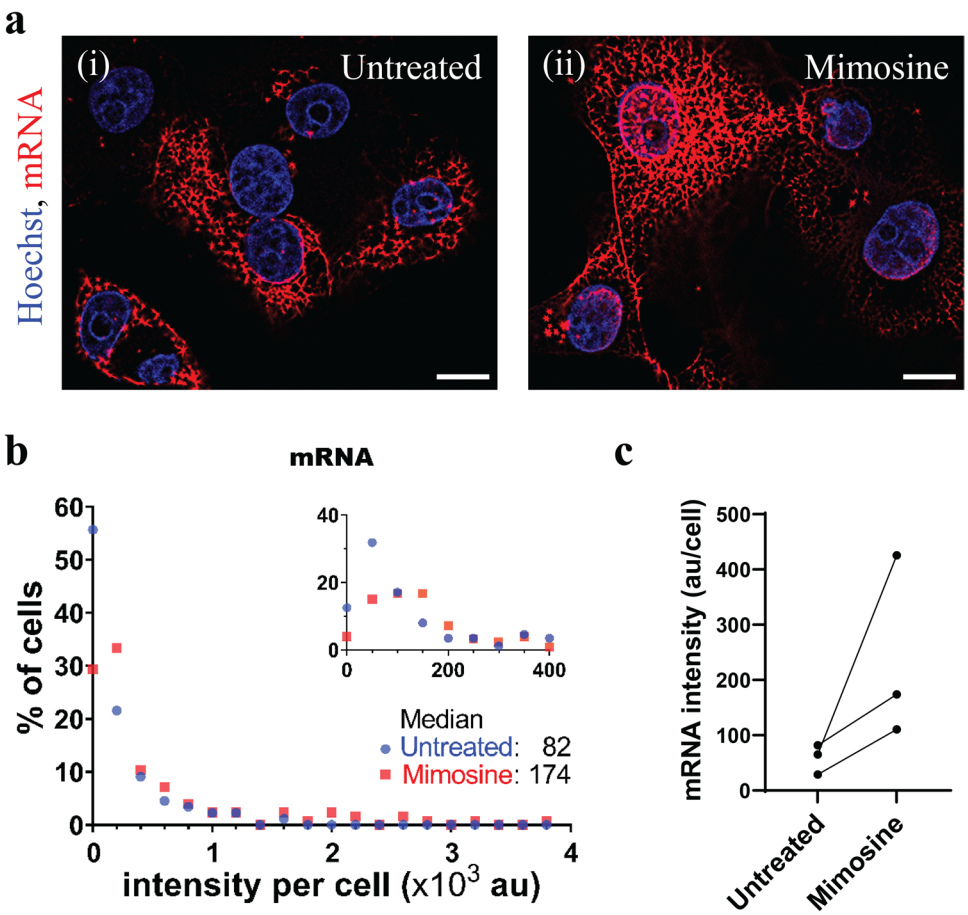

Fig. 9 Quantitative analysis of EGFP transcription in cell-cycle arrested and unarrested cells. The experimental procedures were the same as those described in the legend of Fig. 3, except that the pDNA probe was replaced with the mRNA probe. Stacks of images near the central planes of > 65 cells were captured for each group with a total of 302 mimosine treated cells and 253 untreated cells across 3 independent repeats. **a** Typical fluorescence images of mRNA in (i) untreated cells, and (ii) mimosine arrested cells. The nuclei and EGFP mRNA were labeled with the Hoechst dye (blue) and the mRNA probe (red), respectively. **b** Histograms of mRNA signal intensity per cell in a typical experiment with 200 au bin width (n > 80). The inset shows the same data in a lower intensity range with 50 au bin width. **c** The medians from the histograms in three independent repeats

these cells than unarrested ones, which is consistent with the observation in a previous study that mimosine treatment increases transcriptional activity [6].

The experimental design for comparison of the EGFP protein levels was the same as that for mRNA except that the cells were cultured for 24 h with or without mimosine, instead of 16 h, post electrotransfection. The EGFP level in all samples was quantified by two metrics with flow cytometry: (1) electrotransfection efficiency—the percent of viable cells that were EGFP positive, and (2) expression level per cell—the geometric mean of fluorescence intensity among the EGFP positive cells. For mimosine treated and untreated cells, the mean ± SD of the electrotransfection efficiency were 25 ± 7.9% and 30 ± 3.5%, respectively, and the mean ± SD of the expression level were $3.4 \times 10^5 \pm 0.8 \times 10^5$ arbitrary unit (au) and $3.6 \times 10^5 \pm 0.4 \times 10^5$ au, respectively—neither of these differences were statistically significant (Fig. 10). The lack of significance, despite the relatively large difference at the mRNA level, suggests that either the translation machinery is saturated in both treated and untreated cells, or the treatment decreased the rate of translation. In both cases, the data imply that the decrease in nuclear entry of pDNA

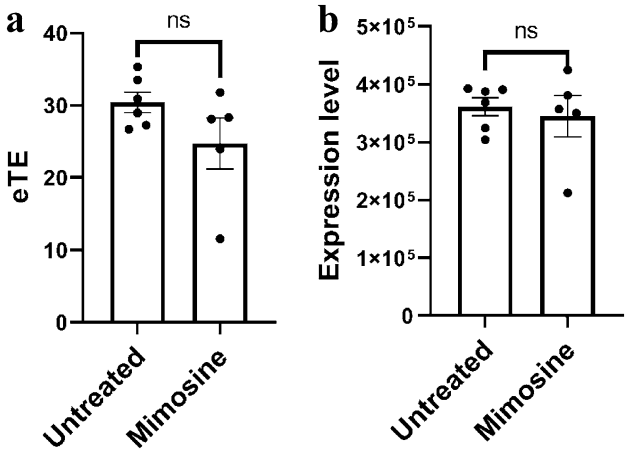

Fig. 10 Transgene expression in cell-cycle arrested and unarrested cells. The experimental procedures were the same as those described in the legend of Fig. 3, except that the transgene expression was quantified at 24 h post electrotransfection. 30,000 Cells were analyzed per group in each experiment. (a) Electrotransfection Efficiency (eTE) - percent of live cells positive for EGFP. **b** Expression Level—geometric mean of EGFP fluorescence intensity among the EGFP positive cells. Symbols represent data points from individual repeats; and bars represent means of the repeats. Error bars, SEM; n = 5–6; ns: non-significant, P > 0.05, Mann–Whitney U test

caused by cell-cycle arrest does not necessarily result in a significant change in protein expression level.

To determine if the observed effects of mimosine treatment on EGFP mRNA and protein levels were the result of broader changes in transcription and translation, total RNA synthesis and total protein level were quantified and compared between mimosine arrested and unarrested cells (Fig. 11). The amount of RNA synthesized was determined by measuring EU incorporation in mimosine treated or untreated cells over a 16-h period in samples with or without continued mimosine treatment. On average, the median level of total RNA synthesis per cell in mimosine treated samples was 0.33 times that in untreated ones (Fig. 11a), indicating that the mimosine treatment decreased RNA synthesis. The total protein content was measured in cells cultured for 48 h with or without mimosine treatment. At the end of the culture, we collected and lysed identical numbers of cells ($>10^6$) in each pair of untreated and mimosine treated samples for protein measurement. On average, the normalized total protein concentration in mimosine treated cells was 0.78 times that in untreated cells (Fig. 11b), indicating that mimosine treatment decreased the total protein concentration as well. The data shown in Fig. 11 were consistent with the previous observations [2], suggesting that mimosine treatment induces different effects on total RNA synthesis and total protein concentration, compared to its impact on transgene expression.

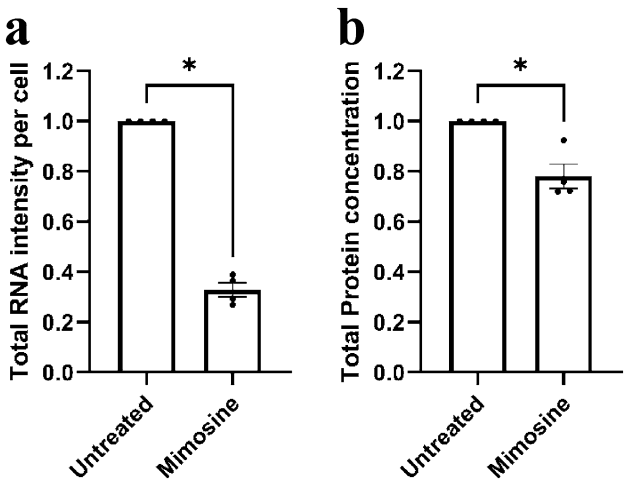

Fig. 11 Effects of mimosine treatment on total RNA synthesis and total protein level. COS7 cells were pretreated with mimosine for 24 h or left untreated, then used for subsequent experiments. **a** Total RNA synthesis. Cells were incubated for 16 h in medium containing 5-ethynyl uridine (EU) and mimosine for cell-cycle arrested cells. For unarrested cells, mimosine was not added to the medium. At the end of the incubation, the total RNA synthesis per cell was quantified in 105–205 cells per group. A total of 536 and 662 cells were analyzed across four independent repeats in untreated and mimosine treated groups, respectively. **b** Total protein level. Cells were incubated for 24 h in medium with or without mimosine, then the BCA assay was performed to quantify total protein level in each sample. $>10^6$ cells were used for each group in four independent repeats. Symbols represent data points from individual repeats; and bars represent means of the repeats. Error bars, SEM; *$P<0.05$; $n=4$; Mann–Whitney U test

Next, we determined if the release of cell-cycle arrest could affect the EGFP protein level. COS7 cells were treated with mimosine for 24 h, followed by electrotransfection of unlabeled pEGFP. Then, the cells were split into two groups, one was continuously treated with mimosine for another 24 h; the other group was released from the treatment in the same period. At the end of the treatment, the EGFP expression was quantified for all samples with flow cytometry. Based on two independent experimental repeats, we calculated the mean ratios between the released and the continuously treated cells for electrotransfection efficiency and expression level per cell, which were 1.3 and 1.1, respectively. The data were consistent with those between untreated and mimosine treated groups (Fig. 10). The comparison suggests that effects of mimosine treatment on transgene expression are reversible, which is similar to the observation on the nuclear entry of pDNA discussed above.

Effects of Mimosine Treatment on Cell Density

COS7 cells were pretreated with mimosine (400 μM, 24 h) or untreated. Then, 1 million cells in each group were electrotransfected with pEGFP and incubated in a medium for another 24 h. The medium was supplemented with nothing (Untreated) or mimosine (400 μM) for continued treatment (Mim). At the end of incubation, the number of cells per unit volume was quantified by flow cytometry. We observed that the cell densities (mean ± SD) were 834,921 ± 176,758 and 51,297 ± 13,408 cells/mL, respectively, in the Untreated and the Mim groups, indicating that mimosine treatment significantly reduced the cell density ($P<0.05$; $n=5$; Mann–Whitney U test). The reduction was a compound effect of increased death and decreased proliferation of cells. We also investigated how the release from cell cycle arrest affected the cell density in two independent repeats. The cells were divided into two groups. In both groups, cells were treated with mimosine for 24 h followed by electrotransfection of pEGFP. Then, cells in the first group were released for 24 h whereas the cells in the second group were continuously treated with mimosine for another 24 h prior to the cell density measurement. The data showed that the mean densities were 72,576 and 41,650 cells/mL in the first and the second groups, respectively, indicating that the release partially recovered the capability of cell division.

Discussion

We investigated DNA electrotransfection in cell-cycle arrested and unarrested cells. Although previous studies have also explored how the arrest influences non-viral

gene delivery [4, 16, 31], this is to our knowledge the first study that performed side-by-side comparison of the levels of intranuclear pDNA in these cells. We observed that the total level was lower in arrested cells than unarrested ones, which was consistent with the previous observation that cell division enhances nuclear entry of electrotransfected pDNA [5, 12, 17], presumably due to the NEBD in dividing cells. Meanwhile, we observed that the nuclear entry of pDNA was not a rare event in cell-cycle arrested cells, presumably due to the active transport through the NPCs. The same phenomenon has also been observed in previous studies [8, 11, 24], particularly for plasmids with a DTS (e.g., SV40). We also observed two distinct patterns of pDNA distribution in the nucleus: diffuse and punctate. Quantitatively, cells subjected to the cell-cycle arrest had a higher level of punctate pDNA and lower level of diffuse pDNA than unarrested cells. In addition to the intranuclear pDNA, the cell-cycle arrest increased the EGFP mRNA level post electrotransfection of pEGFP, but did not change the percent of viable cells positive for EGFP protein or the average EGFP level per cell. These changes in the DNA nuclear entry and transgene expression caused by cell-cycle arrest were reversible after the mimosine treatment was stopped.

The study was accomplished by developing new methods for pDNA detection and image analysis. In previous studies, the detection is often achieved through chemical conjugation of pDNA with a fluorescent dye. At a low molar ratio of dye versus DNA in the conjugate, the fluorescence signal is generally too weak for DNA detection at the single molecule level with fluorescence microscopy; it is only useful for detection of pDNA punctates (see Fig. 7). Increasing the ratio will improve the signal intensity, but may also change DNA's interactions with other biomolecules. For example, the ratio increase can decrease transgene expression, and alter DNA transport in cells [15]. To increase the signal intensity without these consequences, we used a DNA probe to stain the cells post electrotransfection. The new method had a higher sensitivity due to the amplification of the probe signal, allowing us to detect pDNA at the single molecule level, which is critical for the detection of diffuse pDNA in the nuclei. We also developed a method for automatic image analysis that allowed us to analyze a large number of cells, which is hard to achieve through a manual approach. The automatic approach also reduced human errors and ensured robustness, reproducibility, and reliability in the image analysis. With this automated image analysis, we could objectively distinguish pDNA molecules within the nuclei from those in the nuclear envelope or outside the nucleus, distinguish between diffuse and punctate pDNA, and collect a large amount of data for statistical analysis of the samples. The tools developed in the study can also be useful for investigation of gene delivery using other approaches, such as nanoparticles.

We observed two distinct patterns of intranuclear pDNA distribution post electrotransfection: punctate and diffuse. The observation is similar to those in previous studies, following microinjection of DNA into the cytoplasm [8]. Unlike previous studies, we discovered that the diffuse pattern occurred mainly in cells divided post electrotransfection whereas the punctate pattern occurred more in cell-cycle arrested cells. The diffuse pDNA signals are likely to be single molecules spreading throughout the nucleus. The question is, why do some pDNA molecules cluster together to form the punctate structure? Since continuous mimosine treatment increases both punctate pDNA (Fig. 3) and reporter mRNA (Fig. 9) accumulation in electrotransfected cells, we hypothesize that the punctate pDNA is more transcriptionally active than the diffuse pDNA. Thus, the punctates may be the result of multiple pDNA molecules being recruited to hubs of transcription and/or co-transcriptional splicing, which have previously been described and visualized as foci in cell nuclei [21, 28, 29, 33]. Our hypothesis is also in line with recent findings that show another species of circular DNA, extrachromosomal DNA (ecDNA), to form hubs with increased transcriptional activity, facilitated by protein tethering in the nucleus [20, 30, 34]. If the pDNA punctates observed in the current study are hubs of a similar nature, our results suggest that mimosine treatment upregulates their formation or the recruitment of pDNA to existing transcriptional hubs. This hypothesis can explain the observed increase in punctate pDNA and decrease of diffuse pDNA in mimosine treated cells, and is in line with a previous study in which mimosine treatment leads to an increase in transcription of genes with certain promoters [6]. If it can be validated in future studies, facilitating pDNA punctate formation may become a new strategy for improving the efficiency of non-viral gene delivery.

It is well known that the level of a protein is unnecessarily correlated with its mRNA level [18, 23]. However, the correlations among the levels of intranuclear pDNA, mRNA, and protein remain elusive in the field of gene delivery. It has been widely believed that improving the nuclear entry of pDNA will increase transgene expression. Results from our experiments showed an exception since the mimosine treatment decreased intranuclear pDNA level (Fig. 3), but increased mRNA level (Fig. 9) and had insignificant effects on the protein level (Fig. 10), demonstrating that rates of transcription and translation can be influenced by factors independent of the pDNA level in the nucleus. Caution should be exercised when predicting the nuclear entry of pDNA with the data of transgene expression.

Effects of mimosine treatment on cells were reversible in terms of the changes in intranuclear pDNA, transgene expression, and cell proliferation. We observed that mimosine treatment decreased the total and diffuse pDNA signals in the nuclei and the cell density, when comparing to

the untreated cells. The treatment also increased the pDNA punctates in the nuclei. When the cells were released from the treatment for 16 or 24 h, the directions of the changes were reversed, compared to the continuously treated cells, except for the pDNA punctates in the nucleus (see Fig. 6). Instead of decreasing, the release caused either no change or increase in the number of pDNA punctates per nucleus. Our explanation for the observation is as follows. As discussed above, the mimosine treatment might facilitate pDNA transcriptional hub formation via an unknown mechanism. After the treatment was stopped, the hubs would disappear gradually over a certain period rather than instantaneously, and some released cells started to divide, allowing more pDNA molecules to enter the nuclei via the NEBD and reformation. These pDNA could form hubs by the residual effects of the unknown mechanism. As a result, the number of pDNA hubs stayed the same or even increased in the nuclei of released cells.

When the samples were released from the mimosine treatment for 24 h, the cell density was increased by 70%, compared to those continuously treated, although the initial densities of cells in the samples were the same in these groups (10^6 cell/mL). The change was an order of magnitude smaller than the density difference between untreated and continuously treated cells (see the Results section). To explain the large discrepancy, we need to realize that the cell density depends on the difference in rates between cell proliferation and cell death, and the initial density of cells. We observed that the mimosine treatment not only inhibited cell proliferation but also significantly increased cells' vulnerability in electrotransfection. Both events could decrease cell density compared to untreated groups, leading to the large cell density difference. On the other hand, the cells that were released from the mimosine treatment experienced the same increase in cell death upon electrotransfection, compared to continuously treated cells, and regained the proliferation capability afterwards, indicating that the cell density ratio in the two groups depended mainly on the difference between cell proliferation rates rather than the combined effects of cell proliferation and death. Interestingly, the 70% difference in cell density was quantitatively consistent with the observation that ~ 80% of untreated cells divided during a 16-h period (Fig. 2). Thus, the large discrepancy in the cell density data between the untreated group and the group with cell cycle arrested first and then released, is more likely to be due to the difference in cell vulnerabilities to electrotransfection caused by mimosine treatment.

In summary, we developed and validated a sensitive technique for accurate quantification of intranuclear pDNA post electrotransfection. Our data showed that (i) the distribution of pDNA had two different patterns—diffuse and punctate, (ii) cell-cycle arrest decreased the nuclear entry of pDNA, presumably due to the inhibition of NEBD, but also increased the amount of nuclear punctate pDNA and cellular mRNA levels, and (iii) decreasing the nuclear entry did not lead to a reduction in transgene expression. In future studies, we will use the multifaceted approach described herein to evaluate strategies for improving non-viral gene delivery.

Acknowledgments The research was supported partly by Grants from National Institutes of Health (GM130830 and GM145362).

Author Contributions JS: Conceptualization, Methodology, Software, Investigation, Writing—Original Draft Preparation, YW: Methodology (DNA Probe), FY: Supervision, Conceptualization, Writing—Review and Editing.

Data Availability The data that support the findings of this study are available from the corresponding author, FY, upon reasonable request.

Declarations

Conflict of interest All authors declare no competing financial interests that are relevant to the content of this article.

Ethical Approval This study does not involve human or animal subjects.

References

1. Bai, H., G. M. S. Lester, L. C. Petishnok, and D. A. Dean. Cytoplasmic transport and nuclear import of plasmid DNA. *Biosci. Rep.* 37:1–17, 2017. https://doi.org/10.1042/BSR20160616.
2. Basier, C., and P. Nurse. The cell cycle and cell size influence the rates of global cellular translation and transcription in fission yeast. *EMBO J.* 42:e113333, 2023. https://doi.org/10.15252/embj.2022113333.
3. Brunner, S., E. Fürtbauer, T. Sauer, M. Kursa, and E. Wagner. Overcoming the nuclear barrier: cell cycle independent nonviral gene transfer with linear polyethylenimine or electroporation. *Mol. Ther.* 5:80–86, 2002. https://doi.org/10.1006/mthe.2001.0509.
4. Brunner, S., T. Sauer, S. Carotta, M. Cotten, M. Saltik, and E. Wagner. Cell cycle dependence of gene transfer by lipoplex polyplex and recombinant adenovirus. *Gene Ther.* 7:401–407, 2000. https://doi.org/10.1038/sj.gt.3301102.
5. Cervia, L. D., C. C. Chang, L. Wang, M. Mao, and F. Yuan. Enhancing electrotransfection efficiency through improvement in nuclear entry of plasmid DNA. *Mol. Ther. Nucleic Acids*. 11:263–271, 2018. https://doi.org/10.1016/j.omtn.2018.02.009.
6. Chung, L. C., K. H. Tsui, T. H. Feng, S. L. Lee, P. L. Chang, and H. H. Juang. L-mimosine blocks cell proliferation via upregulation of B-cell translocation gene 2 and N-myc downstream regulated gene 1 in prostate carcinoma cells. *Am. J. Physiol. Cell Physiol.* 2012. https://doi.org/10.1152/ajpcell.00180.2011.
7. Colin, M., S. Moritz, P. Fontanges, M. Kornprobst, C. Delouis, M. Keller, A. Miller, J. Capeau, C. Coutelle, and M. Brahimi-Horn. The nuclear pore complex is involved in nuclear transfer of plasmid DNA condensed with an oligolysine–RGD peptide containing nuclear localisation properties. *Gene Ther.* 8:1643–1653, 2001. https://doi.org/10.1038/sj.gt.3301572.
8. Dean, D. A. Import of plasmid DNA into the nucleus is sequence specific. *Exp. Cell Res.* 230:293–302, 1997. https://doi.org/10.1006/excr.1996.3427.
9. Delalande, A., C. Leduc, P. Midoux, M. Postema, and C. Pichon. Efficient gene delivery by sonoporation is associated with

microbubble entry into cells and the clathrin-dependent endocytosis pathway. *Ultrasound Med. Biol.* 41:1913–1926, 2015. https://doi.org/10.1016/j.ultrasmedbio.2015.03.010.
10. Deleage, C., S. W. Wietgrefe, G. Del Prete, D. R. Morcock, X. P. Hao, M. Piatak, J. Bess, J. L. Anderson, K. E. Perkey, C. Reilly, J. M. McCune, A. T. Haase, J. D. Lifson, T. W. Schacker, and J. D. Estes. Defining HIV and SIV reservoirs in lymphoid tissues. *Pathog. Immun.* 1:68–106, 2016. https://doi.org/10.20411/pai.v1i1.100.
11. Dowty, M. E., P. Williams, G. F. Zhang, J. E. Hagstrom, and J. A. Wolff. Plasmid DNA entry into postmitotic nuclei of primary rat myotubes. *Proc. Natl Acad. Sci. USA*. 92:4572–4576, 1995. https://doi.org/10.1073/pnas.92.10.4572.
12. Escriou, V., M. Carriere, F. Bussone, P. Wils, and D. Scherman. Critical assessment of the nuclear import of plasmid during cationic lipid-mediated gene transfer. *J. Gene Med.* 3:179–187, 2001. https://doi.org/10.1002/jgm.174.
13. Ferri, G., G. Fiume, D. Pozzi, G. Caracciolo, and F. Cardarelli. Probing the role of nuclear-envelope invaginations in the nuclear-entry route of lipofected DNA by multi-channel 3D confocal microscopy. *Colloids Surf. B*. 205:111881, 2021. https://doi.org/10.1016/j.colsurfb.2021.111881.
14. Fiume, G., C. Di Rienzo, L. Marchetti, D. Pozzi, G. Caracciolo, and F. Cardarelli. Single-cell real-time imaging of transgene expression upon lipofection. *Biochem. Biophys. Res. Commun.* 474:8–14, 2016. https://doi.org/10.1016/j.bbrc.2016.03.088.
15. Gasiorowski, J. Z., and D. A. Dean. Postmitotic nuclear retention of episomal plasmids is altered by DNA labeling and detection methods. *Mol. Ther.* 12:460–467, 2005. https://doi.org/10.1016/j.ymthe.2005.05.001.
16. Grosjean, F., P. Batard, M. Jordan, and F. M. Wurm. S-phase synchronized CHO cells show elevated transfection efficiency and expression using CaPi. *Cytotechnology*. 38:57–62, 2002. https://doi.org/10.1023/A:1021197830091.
17. Grosse, S., G. Thévenot, M. Monsigny, and I. Fajac. Which mechanism for nuclear import of plasmid DNA complexed with polyethylenimine derivatives? *J. Gene Med.* 8:845–851, 2006. https://doi.org/10.1002/jgm.915.
18. Guo, Y., P. Xiao, S. Lei, F. Deng, G. G. Xiao, Y. Liu, X. Chen, L. Li, S. Wu, Y. Chen, H. Jiang, L. Tan, J. Xie, X. Zhu, S. Liang, and H. Deng. How is mRNA expression predictive for protein expression? A correlation study on human circulating monocytes. *Acta Biochim. Biophys. Sin.* 40:426–436, 2008. https://doi.org/10.1111/j.1745-7270.2008.00418.x.
19. Hagstrom, J. E., J. J. Ludtke, M. C. Bassik, M. G. Sebestyen, S. A. Adam, and J. A. Wolff. Nuclear import of DNA in digitonin-permeabilized cells. *J. Cell Sci.* 110:2323–2331, 1997. https://doi.org/10.1242/jcs.110.18.2323.
20. Hung, K. L., K. E. Yost, L. Xie, Q. Shi, K. Helmsauer, J. Luebeck, R. Schopflin, J. T. Lange, R. Chamorro Gonzalez, N. E. Weiser, C. Chen, M. E. Valieva, I. T. Wong, S. Wu, S. R. Dehkordi, C. V. Duffy, K. Kraft, J. Tang, J. A. Belk, J. C. Rose, M. R. Corces, J. M. Granja, R. Li, U. Rajkumar, J. Friedlein, A. Bagchi, A. T. Satpathy, R. Tjian, S. Mundlos, V. Bafna, A. G. Henssen, P. S. Mischel, Z. Liu, and H. Y. Chang. ecDNA hubs drive cooperative intermolecular oncogene expression. *Nature*. 600:731–736, 2021. https://doi.org/10.1038/s41586-021-04116-8.
21. Jackson, D. A., A. B. Hassan, R. J. Errington, and P. R. Cook. Visualization of focal sites of transcription within human nuclei. *EMBO J.* 12:1059–1065, 1993. https://doi.org/10.1002/j.1460-2075.1993.tb05747.x.
22. Jiang, C., S. P. O'Connor, S. L. Fang, K. X. Wang, J. Marshall, J. L. Williams, B. Wilburn, Y. Echelard, and S. H. Cheng. Efficiency of cationic lipid-mediated transfection of polarized and differentiated airway epithelial cells in vitro and in vivo. *Hum. Gene Ther.* 9:1531–1542, 1998. https://doi.org/10.1089/hum.1998.9.11-1531.
23. Liu, Y., A. Beyer, and R. Aebersold. On the dependency of cellular protein levels on mRNA abundance. *Cell*. 165:535–550, 2016. https://doi.org/10.1016/j.cell.2016.03.014.
24. Ludtke, J. J., M. G. Sebestyén, and J. A. Wolff. The effect of cell division on the cellular dynamics of microinjected DNA and dextran. *Mol. Ther.* 5:579–588, 2002. https://doi.org/10.1006/mthe.2002.0581.
25. Männistö, M., M. Reinisalo, M. Ruponen, P. Honkakoski, M. Tammi, and A. Urtti. Polyplex-mediated gene transfer and cell cycle: effect of carrier on cellular uptake and intracellular kinetics, and significance of glycosaminoglycans. *J. Gene Med.* 9:479–487, 2007. https://doi.org/10.1002/jgm.1035.
26. Motulsky, H. J., and R. E. Brown. Detecting outliers when fitting data with nonlinear regression—a new method based on robust nonlinear regression and the false discovery rate. *BMC Bioinform.* 2006. https://doi.org/10.1186/1471-2105-7-123.
27. Munkonge, F. M., V. Amin, S. C. Hyde, A.-M. Green, I. A. Pringle, D. R. Gill, J. W. S. Smith, R. P. Hooley, S. Xenariou, M. A. Ward, N. Leeds, K.-Y. Leung, M. Chan, E. Hillery, D. M. Geddes, U. Griesenbach, E. H. Postel, D. A. Dean, M. J. Dunn, and E. W. F. W. Alton. Identification and functional characterization of cytoplasmic determinants of plasmid DNA nuclear import. *J. Biol. Chem.* 284:26978–26987, 2009. https://doi.org/10.1074/jbc.m109.034850.
28. Osborne, C. S., L. Chakalova, K. E. Brown, D. Carter, A. Horton, E. Debrand, B. Goyenechea, J. A. Mitchell, S. Lopes, W. Reik, and P. Fraser. Active genes dynamically colocalize to shared sites of ongoing transcription. *Nat. Genet.* 36:1065–1071, 2004. https://doi.org/10.1038/ng1423.
29. Patange, S., D. A. Ball, T. S. Karpova, and D. R. Larson. Towards a 'Spot On' understanding of transcription in the nucleus. *J. Mol. Biol.* 2021. https://doi.org/10.1016/j.jmb.2021.167016.
30. Shaban, H. A., R. Barth, and K. Bystricky. Navigating the crowd: visualizing coordination between genome dynamics, structure, and transcription. *Genome Biol.* 21:278, 2020. https://doi.org/10.1186/s13059-020-02185-y.
31. Tseng, W. C., F. R. Haselton, and T. D. Giorgio. Mitosis enhances transgene expression of plasmid delivered by cationic liposomes. *Biochim. Biophys. Acta Gene Struct. Expr.* 1445:53–64, 1999. https://doi.org/10.1016/S0167-4781(99)00039-1.
32. Wang, F., J. Flanagan, N. Su, L. C. Wang, S. Bui, A. Nielson, X. Wu, H. T. Vo, X. J. Ma, and Y. Luo. RNAscope: a novel in situ RNA analysis platform for formalin-fixed, paraffin-embedded tissues. *J. Mol. Diagn.* 14:22–29, 2012. https://doi.org/10.1016/j.jmoldx.2011.08.002.
33. Yano, K.-I., L. Rems, T. Kotnik, D. Miklavcic, J. Weaver, K. Smith, R. Son, T. Gowrishankar, P. Vernier, Z. Levine, M.-P. Rols, J. Teissie, L. Mir, A. Pakhomov, P. Nick, W. Frey, D. Dean, K. Morotomi-Yano, R. Neal, and S. Beebe. Chapter 4: biological responses. In: Bioelectrics, edited by H. Akiyama, and R. Heller. Tokyo: Springer, 2017, pp. 155–274.
34. Yi, E., A. D. Gujar, M. Guthrie, H. Kim, D. Zhao, K. C. Johnson, S. B. Amin, M. L. Costa, Q. Yu, S. Das, N. Jillette, P. A. Clow, A. W. Cheng, and R. G. W. Verhaak. Live-cell imaging shows uneven segregation of extrachromosomal DNA elements and transcriptionally active extrachromosomal DNA hubs in cancer. *Cancer Discov.* 12:468–483, 2022. https://doi.org/10.1158/2159-8290.CD-21-1376.